High-Cycle Fatigue of Nickel-Based Superalloy ME3 at Ambient and Elevated Temperatures: Role of Grain-Boundary Engineering

YONG GAO, MUKUL KUMAR, R.K. NALLA, and R.O. RITCHIE

High-cycle fatigue (HCF), involving the premature initiation and/or rapid propagation of cracks to failure due to high-frequency cyclic loading, remains a principal cause of failures in gas-turbine propulsion systems. In this work, we explore the feasibility of using "grain-boundary engineering" as a means to enhance the microstructural resistance to HCF. Specifically, sequential thermomechanical processing, involving alternate cycles of strain and annealing, was used to increase the fraction of "special" grain boundaries and to break up the interconnected network of "random" boundaries, in a commercial polycrystalline Ni-based superalloy (ME3). The effect of such grain-boundary engineering on the fatigue-crack-propagation behavior of large (~8 to 20 mm), through-thickness cracks at 25 °C, 700 °C, and 800 °C was examined. Although there was little influence of an increased special boundary fraction at ambient temperatures, the resistance to near-threshold crack growth was definitively improved at elevated temperatures, with fatigue threshold stress intensities some 10 to 20 pct higher than at 25 °C, concomitant with a lower proportion (~20 pct) of intergranular cracking.

I. INTRODUCTION

NICKEL-BASED superalloys are widely used in turbines for both aerospace and land-based power-generation applications, due to their exceptional elevated-temperature strength, high resistance to creep, oxidation, and corrosion, and good fracture toughness. However, a critical property of these alloys is their resistance to fatigue-crack propagation, particularly at service temperatures. In engine applications, there are often two components to this problem: (1) low-cycle fatigue, which results from relatively large cycles associated with the stopping and starting of the turbine, and (2) high-cycle fatigue (HCF), associated with vibrational loading during service. The HCF, in particular, has been recognized as the single largest cause of engine failures in military aircraft.[1] It results in rapid, and often unpredictable, failures due to the propagation of fatigue cracks in blade and disk components under high-frequency loading, where the cracking initiates from small defects, in many instances resulting from fretting or foreign-object damage.[2] Due to the high vibrational frequencies involved, even cracks growing at slow per-cycle velocities can propagate to failure in short time periods, possibly within a single flight segment. Consequently, HCF-critical turbine-engine components must be operated below the fatigue-crack initiation or growth thresholds, such that cracking cannot occur within $\sim 10^9$ cycles. To address this problem, significant research efforts have been directed in recent years to developing HCF design and life-prediction methodologies for titanium- and nickel-based alloys; these studies have resulted in an extensive database on HCF,[1,3,4] which has been exclusively directed to typical blade and disk microstructures.[5–8] However, the question as to whether these microstructures can be optimized to promote HCF resistance has rarely been addressed.

One approach to enhancing microstructural resistance to fracture has been through the notion of grain-boundary engineering, where the "character" of the grain boundaries is changed by thermomechanical treatment.[9] Specifically, the grain-boundary character distribution (GBCD) is controlled principally by promoting a high proportion of so-called "special" grain boundaries. These boundaries are characterized by a particular misorientation and high degree of atomic matching; they are described geometrically by a low "sigma number" ($1 < \Sigma \leq 29$), which is defined in terms of the coincident-site lattice (CSL) model[10] as the reciprocal of the fraction of lattice points in the boundaries that coincide between the two adjoining grains, with an allowable angular deviation from the Brandon criterion of $\Delta\theta \leq 15 \text{ deg} \cdot \Sigma^{-1/2}$.[11] Processing generally involves several strain-annealing cycles to induce (1) strain by cold working and (2) strain-induced grain-boundary migration during subsequent annealing, the latter creating special grain boundaries *via* a boundary decomposition mechanism in the grain-boundary network.[12] In addition to an enhanced fraction of special boundaries, such "engineered" microstructures can possess a refined grain size and diminished incidence of deviation from the exact Σ misorientations; the texture, however, generally remains unchanged or, in some cases, can be reduced.

To date, the grain-boundary engineering approach has been shown to be particularly successful in promoting fracture resistance in specific cases, notably in the context of intergranular stress-corrosion cracking[13–20] and creep[21–24]. However, its effect on the fatigue resistance has largely been unexplored; indeed, to our knowledge, only one such study exists in archival literature.[25] In that study, ambient-temperature, smooth-bar, tension-tension fatigue lives for two γ/γ' superalloys were reported to be increased by a factor of ~1.5 in an Fe-based alloy by increasing the fraction

YONG GAO, Graduate Student, and R.O. RITCHIE, Professor, are with the Department of Materials Science and Engineering, University of California, Berkeley, CA 96720. Contact e-mail: roritchie@lbl.gov MUKUL KUMAR, Member of the Scientific Staff, is with the Lawrence Livermore National Laboratory, Livermore, CA 94550. R.K. NALLA, Postdoctoral Research Fellow, is with the Materials Science Division, Lawrence Berkeley National Laboratory, Berkeley, CA 94720.

Manuscript submitted April 7, 2005.

of special boundaries from 20 to 65 pct and by a factor of 3 in a Ni-based alloy by increasing this fraction from 9 to 49 pct, although no mechanistic explanation was presented.

Clearly, the effectiveness of grain-boundary engineering will depend upon the nature of the crack path, specifically, the preponderance of intergranular *vs* transgranular cracking. In light of this, the objective of the present study was to investigate, for the first time, the feasibility of using grain-boundary engineering processing to promote resistance to fatigue-crack propagation, particularly at near-threshold levels, in a new polycrystalline nickel-based disk alloy, ME3. Specifically, the crack growth rates and threshold behavior of large (8 to 20 mm) through-thickness cracks were examined over a range of temperatures (25 °C, 700 °C, and 800 °C) in order to enhance the incidence of intergranular crack growth.

II. EXPERIMENTAL PROCEDURES

A. *Materials*

An advanced powder-metallurgy nickel-based superalloy, ME3, was used in this study. It is a relatively new polycrystalline Ni-Co-Cr alloy, of proprietary chemical composition (similar to Udimet 720), designed to have extended durability at 650 °C for aircraft engine disk applications by utilizing a moderately high γ' precipitate content with high refractory-element levels. Forged heats of the alloy were received as plate stock from General Electric (GE) Aircraft Engines (fine-grained sample) and from NASA–Glenn (coarse-grained sample). The as-received microstructure comprised a bimodal distribution of ~20 nm and 100 to 200 nm ordered γ' ($L1_2$) precipitates within the equiaxed γ matrix, as described by Nembach and Neite.[26] The matrix grain size (d_g), was 1.3 and 15 μm in the two as-received conditions for the GE and NASA heats, respectively. Typical ambient- and elevated-temperature mechanical properties are listed in Table I.[27]

B. *Thermomechanical Treatments*

To vary the GBCD, the effects of several thermomechanical processing parameters were first evaluated, including prestrain (by cold rolling), annealing time, and temperature. Based on earlier grain-boundary engineering processing of INCONEL* 600,[24] cold rolling was used to vary the prestrain from 5 to 20 pct, followed by annealing at temperatures from 1000 °C to 1170 °C with annealing times of 15 to 45 minutes; in addition, air cooling instead of water or oil quenching was adopted to avoid quench cracking. Based on a series of preliminary multiparametric optimization tests, the following processing sequence was adopted to promote a high fraction of special grain boundaries.

(1) As-received plates were electrodischarge machined into 35 × 30 × 15 mm sections.
(2) Sections were solutionized at 1175 °C for 1 to 2 hours, followed by an air cool to room temperature to dissolve the γ' precipitates.
(3) Microstructures were then grain-boundary engineered using four cycles of strain and high-temperature annealing of the single-phase alloy, specifically involving cycles of cold rolling (10 pct reduction in thickness per cycle) followed by a 30-minute anneal at 1150 °C in an air furnace.
(4) Finally, a duplex aging treatment (4 hours at 843 °C, followed by 8 hours at 760 °C) was carried out to reprecipitate the γ' as a bimodal distribution of cuboidal precipitates.

Additionally, to compare with the as-received and grain-boundary engineered microstructures, some as-received sections from the fine-grained heat were grain-coarsened by heat-treating for 3.5 hours at 1175 °C; this heat treatment led to little or no change in the GBCD compared to the as-received material.

*INCONEL is a trademark of INCO Alloys International, Huntington, WV.

Table I. Typical Mechanical Properties of the As-Received ME3 Alloy at Ambient and Elevated Temperatures for the Initially Fine-Grained and Coarse-Grained Heats

Temperature (°C)	Yield Strength (MPa)	Ultimate Strength (MPa)	Reduction in Area
25 (fine)	1180	1620	26 pct
700 (fine)	1040	1300	18 pct
25 (coarse)	1150	1650	21 pct
700 (coarse)	980	1310	15 pct
800 (coarse)	900	980	12 pct

C. *Large-Crack Propagation Tests*

The fatigue-crack-propagation behavior of large (~8 to 20 mm) through-thickness cracks in the as-received, grain-boundary-engineered, and grain-coarsened microstructures was characterized in air at ambient (25 °C) and elevated (700 °C and 800 °C) temperatures using 6- to 8-mm-thick, 25.4-mm-wide, compact-tension (C(T)) specimens of the as-received microstructures, all machined with the crack plane perpendicular to the circumferential direction and crack growth in the radial direction (the C-R orientation). However, after grain-boundary engineering, the (C(T)) specimens can be considered to be in the L-T orientation, *i.e.*, with the crack plane perpendicular to the rolling direction (L) and crack growth in the transverse direction (T). Testing was performed on computer-controlled, servohydraulic testing machines (MTS Systems Corp., Eden Prairie, MN), in general accordance with ASTM Standard E-647,[28] with specimens cycled under stress-intensity (K) control, at frequencies between 10 and 25 Hz (sine wave) at a load ratio (ratio of minimum to maximum loads) of $R = 0.1$. Fatigue thresholds (ΔK_{TH}), defined as the minimum stress-intensity range to yield a growth rate of 10^{-10} m/cycle, were approached using automated load-shedding at a normalized K gradient of -0.08 mm^{-1}, as specified in the standard. Multisample tests were conducted to verify the effect of grain-boundary engineering on the large-crack propagation behavior; specifically, at least three samples were tested for each microstructural condition, and in each sample, growth rates were determined under both decreasing- and increasing-K conditions.

Crack-length measurements at all temperatures were determined from the unloading elastic compliance, as measured by a capacitance gage (Model HPT-150E-S-N2-3-B,

Capacitec, Ayer, MA) mounted across the notch mouth. Stress intensities were determined from the linear-elastic solutions for the (C(T)) geometry given in ASTM Standard E-399.[29] For all tests and conditions, the specimen thickness (B), width (W), and crack length (a) were always large compared to the maximum plastic-zone size, estimated by $r_{y,\max} \sim 1/2\pi (K_{\max}/\sigma_y)^2$, where $K_{\max}$ is the maximum stress intensity in the fatigue cycle and σ_y is the yield strength; specifically, B, W, and $a > 15r_{y,\max}$, implying that plane-strain, small-scale yielding conditions prevailed throughout. Results are presented in terms of the crack growth rate per cycle (da/dN) as a function of the applied stress-intensity range (ΔK).

D. *Electron Backscattered Diffraction Characterization*

Electron backscattered diffraction (EBSD) provides the best method to measure the grain-boundary character and the triple-junction distributions. These measurements were made, along with the crystallographic texture, by orientation mapping of metallographically prepared specimens in a PHILIPS* XL-30S scanning electron microscope (SEM) equipped with the OIM** software from TSL, Inc. Analysis of the EBSD data was performed using custom algorithms described in detail elsewhere.[30,31,32] Grain boundaries were categorized according to the coincident-site lattice model and the Brandon criterion.[10,11] In all cases, the EBSD characterization was performed at the center of the sample in a plane perpendicular to the rolling direction; the scanned areas were typically 1-mm square and always encompassed in excess of 2000 analyzed grain boundaries.

*PHILIPS is a trademark of Philips Electronic Instruments Corp., Mahwah, NJ.

**OIM is a trademark of TSL, Inc., Draper, UT.

III. RESULTS AND DISCUSSION

A. *Grain-Boundary Characterization*

The EBSD results on the GBCD and texture of the as-received and grain-boundary-engineered microstructures are given in Figure 1; both the fine-grained (GE sample) and coarse-grained (NASA sample) as-received and grain-boundary-engineered structures are shown. In this figure, the random grain boundary network is enhanced in black and the special grain boundaries are in color, with red representing $\Sigma 3$ (twin) boundaries and yellow representing other $\Sigma 3^n$ special boundaries. The corresponding characteristics of all microstructures, including the grain-coarsened structure, are listed in Table II. It should be noted that, barring the grain size, the characteristics of the fine- and coarse-grained materials are essentially the same.

For both alloys, the (number) fraction of special grain boundaries (f_N) in the as-received condition constitutes no more than 29 pct of the total number of boundaries. After grain-boundary engineering, however, this "special fraction" by number was increased to 41 to 42 pct.* With respect to grain size, the coarse-grained alloy remained effectively unchanged after the grain-boundary engineering processing, whereas the initially fine-grained alloy showed grain coarsening from an average of 1.3 to 13 μm. Additional EBSD scans verified that these microstructures were isotropic, regardless of the plane of observation.

Specifically, grain-boundary engineering resulted in an increase in the number fraction of special boundaries, from 0.29 to 0.42 and from 0.28 to 0.41 in the fine- and coarse-grained alloys, respectively. Additionally, the length fractions (f_L) of special boundaries were correspondingly increased in the two alloys from 0.36 to 0.57 and 0.38 to 0.56. The disproportionate increase in the length fraction in comparison with the number fraction (f_N) is entirely due to the increased frequency of lower-energy special boundaries like annealing twins ($\Sigma 3$). With an increase in the fraction of special boundaries, there was also a marked reduction in the fraction of triple junctions that are coordinated with three crystallographically random boundaries (J_o),** accompanied by an increase in the fraction of J_3 junctions, where three special boundaries are coordinated. Indeed, the listed ratio, $J_2/(1 - J_3)$, has been related to the probability of crack arrest for fracture mechanisms involving intergranular crack propagation.[30,32]

Another important effect of grain-boundary engineering was seen in the cluster mass distribution* in the manner of References 32 and 33. Over 95 pct of the random boundaries in the as-received microstructures were in clusters larger than 500 grain diameters, which implies that the network of random boundaries was infinite in extent. This percentage was reduced to zero in the grain-boundary-engineered microstructures, indicating that an infinitely percolating network of random boundaries did not exist in the engineered microstructures, even with only a modest enhancement in the fraction of special boundaries.

All microstructures (except the as-received fine-grained alloy with $d_g \sim 1.3$ μm) revealed no change in hardness (Rockwell C $\sim$ 44) after the grain-boundary engineering processing. Additionally, they displayed very low texture, *i.e.*, $\sim$1.5 to 1.7 times random; this can be categorized as weak to no texture, but is indicative of an fcc alloy with low stacking-fault energy. Specifically, only a minimal $<111>$ component was apparent in all as-received and grain-boundary-engineered structures (Figure 1).

Grain coarsening by annealing at 1175 °C (for 3.5 hours) of the (initially) fine-grained alloy resulted in an increase in grain size from 1.3 to 17 μm, although the special grain-boundary fraction remained essentially the same as the as-received microstructure; the texture (or lack thereof) was also unchanged. It is interesting to note, however, that the length fraction of special boundaries was $\sim$0.15 higher in the grain-coarsened structure, due to the comparatively longer twin boundaries ($\Sigma 3$) in the coarser microstructure after grain growth.

*This increase in the fraction of special boundaries with grain-boundary engineering is significantly higher than that reported for other two-phase austenitic alloys.[25]

**J_n refers to the fraction of triple points that have n special boundaries, where n = 0, 1, 2, or 3.

*A cluster is described as a microstructural entity composed entirely of contiguous special or random boundaries, and its scalar dimension can be quantified from the EBSD data.

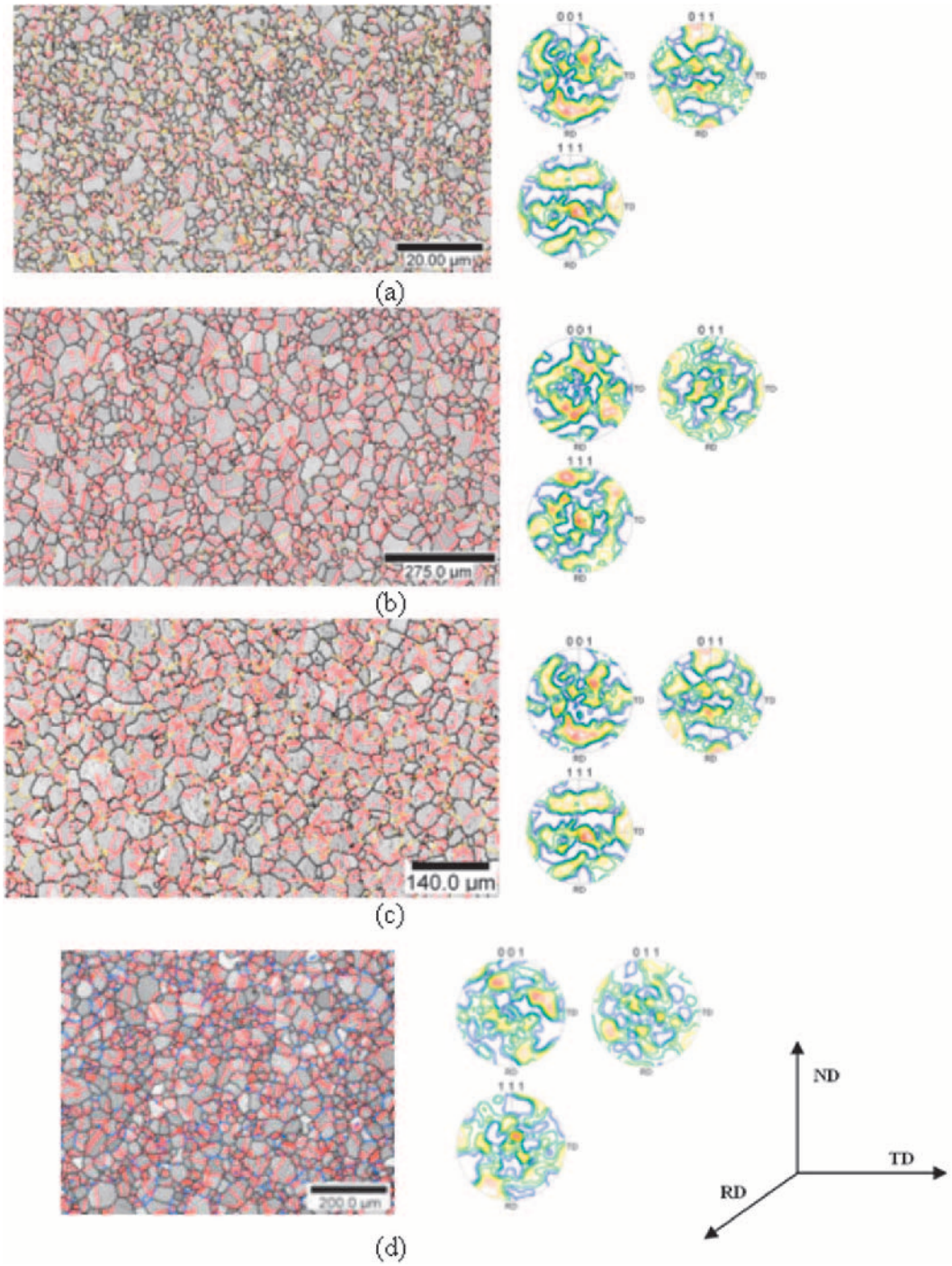

Fig. 1—GBCD and texture pole figures, derived using EBSD for the ME3 alloy in the (*a*) as-received fine-grained (GE) condition, (*b*) as-received coarse-grained (NASA) condition, (*c*) grain-boundary-engineered (fine-grained) condition, and (*d*) grain-boundary-engineered (coarse-grained) condition (for the plane perpendicular to the rolling direction). Random boundaries are shown as black lines and special boundaries are in color (red ≡ Σ3 (twin) and yellow ≡ $\Sigma 3^n$ special boundaries). The {001}, {011}, and {111} pole figures, showing the rolling (RD), transverse (TD), and normal (ND) directions, were also generated from the EBSD data.

B. *Fatigue-Crack-Propagation Behavior*

1. *Ambient temperatures*

The variation in the fatigue-crack-propagation rates of large (~8 to 20 mm), through-thickness cracks in the as-received, grain-boundary-engineered, and grain-coarsened microstructures in ME3 at 25 °C (with $R = 0.1$) are shown in Figure 2 as a function of the stress-intensity range. The most striking feature of these results is the marked influence of grain size; values of the ΔK_{TH} fatigue thresholds, listed in Table III, increase linearly from 5.6 MPa$\sqrt{\text{m}}$ for a 1.3 μm grain size (as-received, fine-grained alloy) to 11.5 MPa$\sqrt{\text{m}}$ for a 17 μm grain size (grain-coarsened alloy), as shown in Figure 3. However, when compared at comparable grain sizes (~13 to 15 μm), it is clear that there

Table II. Microstructural Parameters for ME3 Alloy Microstructures in the As-Received, Grain-Boundary-Engineered, and Grain-Coarsened Conditions

Characteristics	As-Received (Fine-Grained)	As-Received (Coarse-Grained)	GB Engineered (Fine-Grained)	GB Engineered (Coarse-Grained)	Grain-Coarsened
Average grain size (μm)	1.3	15	13	16	17
Grain-size range (μm)	0.5 to 6.5	4 to 77	3 to 60	5 to 100	4 to 72
Special length fraction (f_L)	0.36	0.38	0.57	0.56	0.50
Special number fraction (f_N)	0.29	0.28	0.42	0.41	0.30
Triple-junction distribution	$J_0 = 0.32$	$J_0 = 0.34$	$J_0 = 0.17$	$J_0 = 0.16$	$J_0 = 0.27$
	$J_1 = 0.51$	$J_1 = 0.51$	$J_1 = 0.56$	$J_1 = 0.56$	$J_1 = 0.57$
	$J_2 = 0.13$	$J_2 = 0.12$	$J_2 = 0.12$	$J_2 = 0.11$	$J_2 = 0.10$
	$J_3 = 0.04$	$J_3 = 0.03$	$J_3 = 0.15$	$J_3 = 0.17$	$J_3 = 0.06$
$J_2/(1 - J_3)$*	0.135	0.124	0.141	0.133	0.106
Texture (times random)	1.5 (very weak)	1.6 (very weak)	1.5 (very weak)	1.7 (very weak)	1.6 (very weak)
Cluster mass (random boundary network)	90 pct > 1000	90 pct > 500	80 pct > 500	—	—

*J_n refers to the fraction of triple junctions that have n special grain boundaries.

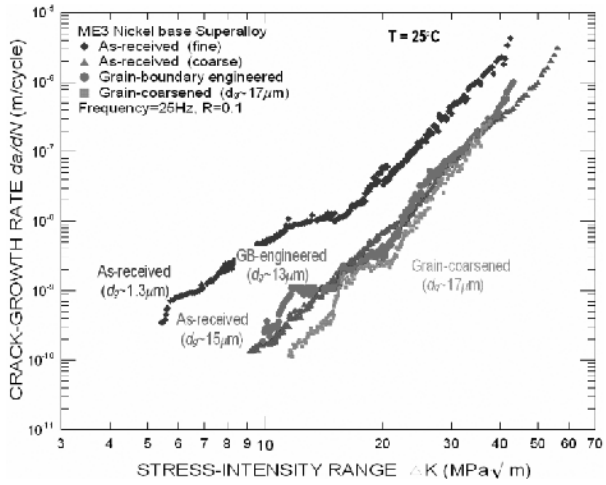

Fig. 2—Fatigue-crack propagation rates at 25 °C for large (~8 to 20 mm) cracks in the nickel-based superalloy ME3, as a function of the stress-intensity range, for the as-received, grain-boundary-engineered, and grain-coarsened microstructures. Note the large effect of grain size on near-threshold behavior.

Table III. Large-Crack Fatigue Thresholds (in MPa$\sqrt{\text{m}}$), Measured at $R = 0.1$ at Ambient and Elevated Temperatures

Temperatures (°C)	As-Received (Fine-Grained)	As-Received (Coarse-Grained)	Grain-Boundary Engineered	Grain-Coarsened
25	5.4	9.3	9.8	11.5
700	—	8.1	9.0	—
800	—	9.3	11.2	—

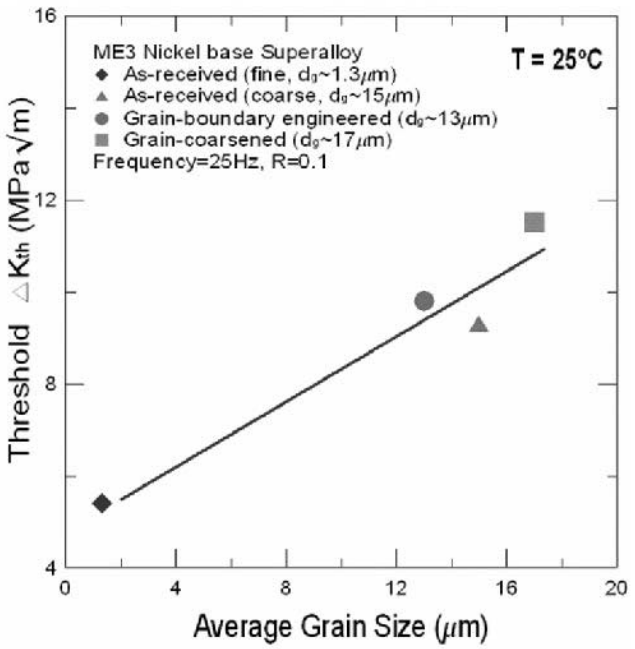

Fig. 3—Relationship between measured fatigue thresholds (at $R = 0.1$) and the average grain size for the ME3 superalloys at ambient temperatures.

is little independent effect of grain-boundary engineering on fatigue-crack propagation and threshold behavior at ambient temperatures. The ΔK_{TH} thresholds are comparable (within 5 pct) for the as-received coarse-grained (with $f_N \sim 0.28$) and grain-boundary-engineered (with $f_N \sim 0.42$) structures, despite an ~50 pct increase in the special grain-boundary fraction; furthermore, they are ~17 pct higher in the grain-coarsened microstructure (where $f_N \sim 0.30$).

The absence of an effect of grain-boundary engineering at 25 °C is consistent with the observed mechanisms of crack extension at this temperature. The SEM fractography of the fatigue surfaces in the as-received and grain-boundary-engineered microstructures, shown in Figures 4(a) and (b) at near-threshold levels and in Figures 4(c) and (d) at higher growth-rate behavior, reveal a predominantly transgranular cracking mode. Typical of many superalloys with low stacking-fault energy,[26] such transgranular crack growth was highly planar and often crystallographic in character, with the facets on the fracture surfaces consistent with slip along the {111} planes (Figure 4). Indeed, the transition

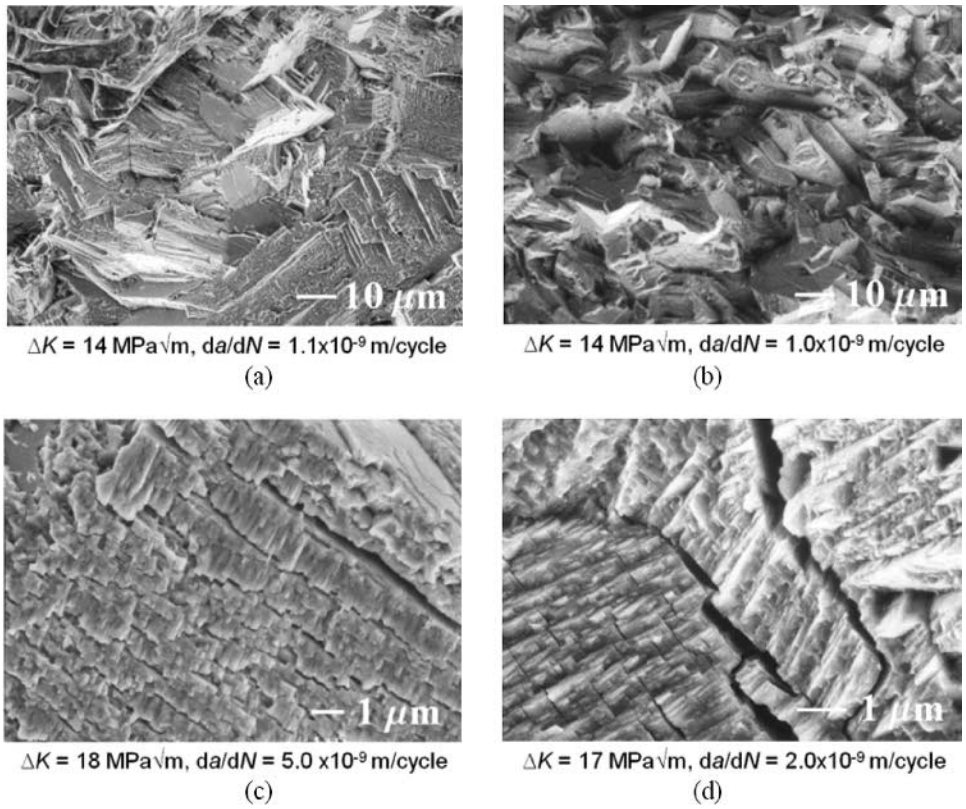

Fig. 4—SEM fractography of ambient-temperature fatigue-crack propagation in ME3 at near-threshold stress intensities, for the (*a*) and (*c*) as-received microstructure and (*b*) and (*d*) grain-boundary-engineered microstructure. Crack is propagating from left to right.

to this faceted, crystallographic mode occurred in both microstructures when the cyclic plastic-zone size ($r_y \sim 1/2\pi(\Delta K/2\sigma_y)^2$) approached the average grain size, *i.e.*, approximately when $\Delta K < 10$ to 12 MPa$\sqrt{\text{m}}$. Consequently, as cracks propagated transgranularly in ME3 at ambient temperatures, it is unlikely that changing the character of the grain boundaries, by increasing the special fraction, would have a significant effect on crack-growth resistance.

Similar results have been obtained for the ambient-temperature behavior of small (~10 to 900 μm) surface fatigue cracks in the as-received and grain-boundary engineering microstructures of ME3, where crack extension was predominantly transgranular.[34] What is important to note here is that irrespective of the size of the cracks relative to the scale of microstructure, where the crack path is transgranular, there is little discernable effect of an increased fraction of special boundaries on the ambient-temperature crack-growth resistance of fatigue-crack growth in ME3.

2. *Elevated temperatures*

To evaluate the effect of grain-boundary engineering at elevated temperatures, which are more representative of the practical applications for this alloy, large-crack fatigue-crack growth-rate data for the as-received and the grain-boundary-engineered microstructures of similar average grain sizes (13 to 15 μm) were compared at 700 °C and 800 °C with growth-rate data at 25 °C. The results, shown in Figure 5, indicate that crack-growth rates in both microstructures are typically faster by one to two orders of magnitude at 700 °C to 800 °C than at ambient temperature. More importantly, although there is no difference in behavior above $\sim 10^{-7}$ m/cycle, there is a definitive, albeit small, increase in crack-growth resistance in the grain-boundary-engineered microstructures at near-threshold levels, below $\sim 10^{-7}$ m/cycle. Specifically, with the increase in fraction of special boundaries, near-threshold growth rates (at a specific ΔK level) are some 5 to 10 times lower, and the ΔK_{TH} thresholds are ~10 pct higher at 700 °C and over 20 pct higher at 800 °C, as compared to values at ambient temperature (Table III).

This beneficial effect of grain-boundary engineering at elevated temperatures can also be traced to the mechanisms of cyclic crack extension. Crack-path profiles at 700 °C, imaged in the SEM, show how the crack path at near-threshold levels is highly faceted, as at ambient temperatures, but now involves some intergranular crack propagation, since the grain boundaries can act as preferential paths for the diffusion of oxygen and for crack advance.[35] At higher growth rates, however, crack paths cease to be faceted and revert to a fully transgranular mode (Figure 6). This transition again occurs when the plastic-zone size becomes much larger than the grain size.

Quantitatively, the proportion of intergranular fracture could be best determined from area fractions on lower-magnification SEM fractographs. As shown in Figure 7, near-threshold fatigue-crack growth in ME3 is characterized by an increasing proportion of intergranular cracking with increase in temperature. Measurements on the as-received material at $\Delta K \sim 10$ MPa$\sqrt{\text{m}}$ revealed an area fraction of intergranular facets of ~40 pct at 700 °C and as high as ~75 pct at 800 °C. Most importantly,

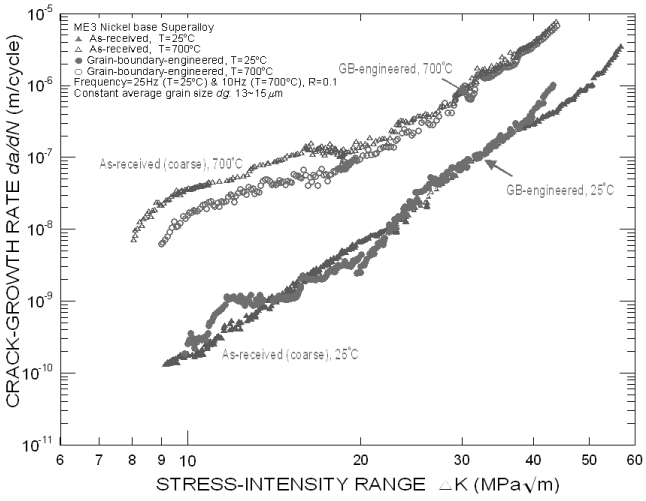

(a)

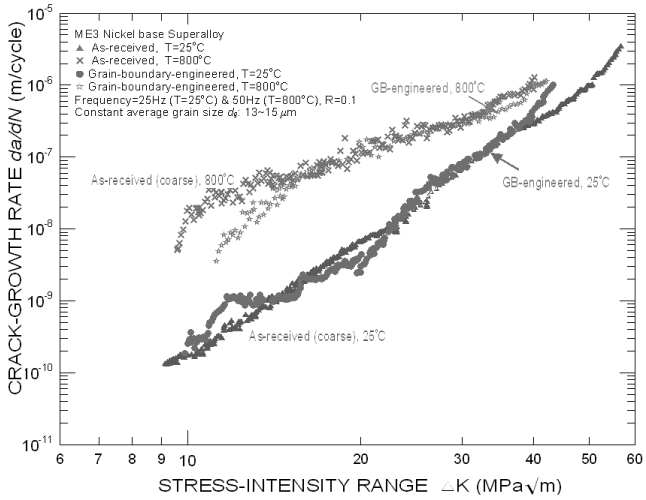

(b)

Fig. 5—Fatigue-crack-propagation behavior at elevated temperatures for large (~8 to 20 mm) cracks in ME3, as a function of the stress-intensity range, for the as-received and grain-boundary-engineered microstructures. Shown are results at (*a*) 700 °C and (*b*) 800 °C, as compared to the behavior at 25 °C.

however, after increasing the fraction of special boundaries by grain-boundary engineering, there was a definite reduction in the relative proportion of intergranular crack growth, specifically by some 20 to 25 pct (Figure 8).

Accordingly, as shown in Figure 9 by the increase in ΔK_{TH} thresholds with increasing fraction of special grain boundaries, it does appear that, due to the presence of intergranular cracking during near-threshold crack growth in ME3 at elevated temperatures (700 °C to 800 °C), there is a positive effect of grain-boundary engineering, independent of any change in grain size, in improving the resistance to fatigue-crack growth, specifically in the critical low-growth-rate regime which often controls the overall life of a structure.

The precise reason why the presence of a higher fraction of special boundaries leads to a reduction in the incidence of intergranular crack growth is not known, but it seems reasonable to presume that the effect is primarily associated with their enhanced fracture resistance, especially in the presence of a high-temperature oxidizing environment, which results in a higher proportion of transgranular cracking.

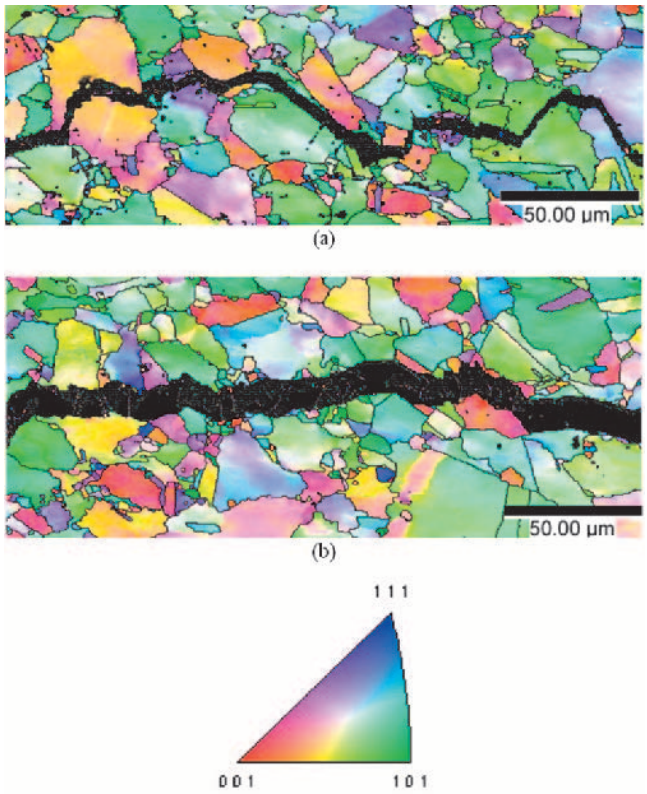

Fig. 6—EBSD maps of the fatigue-crack paths in the grain-boundary-engineered ME3 microstructure tested at 700 °C, showing behavior (*a*) at lower growth rates ($\Delta K \sim 12$ MPa$\sqrt{\text{m}}$) and (*b*) at higher growth rates ($\Delta K \sim 24$ MPa$\sqrt{\text{m}}$). Note that as these two micrographs were taken from the same specimen, which was cycled under decreasing-ΔK conditions, the crack-opening displacement was larger for the higher growth-rate profile (Figure 6(b)), as this region was further away (10 mm) from the crack tip when the image was taken. Crack is propagating from left to right. (Image courtesy of V. Radmilovic.)

Indeed, studies of environmentally assisted intergranular cracking[13–20] and high-temperature creep[21–24] have all demonstrated the superior fracture resistance of these boundaries. However, their presence may also modify dislocation behavior, for example, by acting as a source or sink of incoming mobile dislocations. This could indirectly result in more aggregation of dislocations near the boundary, particularly as there is less free volume in special (as compared to random) boundaries, thereby strengthening the boundary region. This effect has been observed locally near individual boundaries by Alexandreanu *et al.*,[36] and the effect of an increased special fraction on the constitutive response has been documented by Kumar *et al.*[37]

IV. CONCLUSIONS

Based on an investigation into the feasibility of using grain-boundary engineering by strain/anneal cycling to promote the high-cycle fatigue-crack-propagation resistance of the powder-metallurgy polycrystalline nickel-based superalloy ME3 in ambient- to elevated- (700 °C to 800 °C) temperature air environments, the following conclusions can be made.

1. Using grain-boundary engineering techniques involving several cycles of strain (10 pct cold rolling) and high-temperature

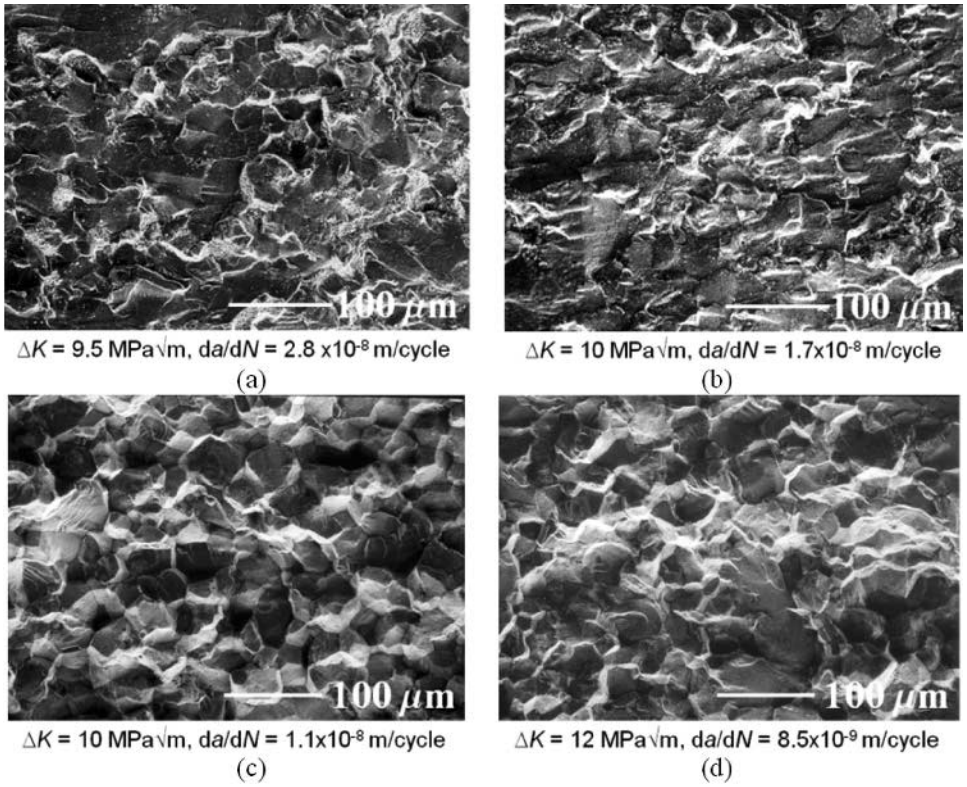

Fig. 7—SEM fractography of near-threshold fatigue-crack growth at elevated temperatures in ME3, showing a comparison between (*a*) the as-received microstructure at 700 °C, (*b*) the grain-boundary-engineered microstructure at 700 °C, (*c*) the as-received microstructure at 800 °C, and (*d*) the grain-boundary-engineered microstructure at 800 °C. Note the lower proportion of intergranular fracture in the grain-boundary-engineered microstructures. Crack is propagating from left to right.

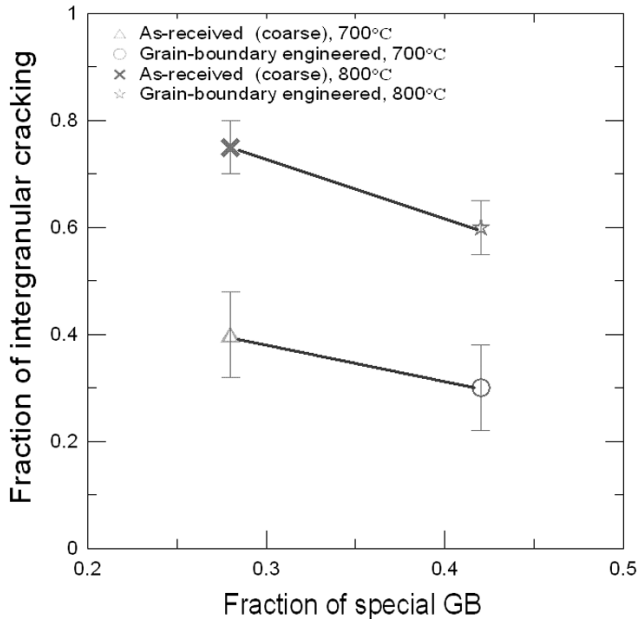

Fig. 8—Relationship between the fraction of special grain boundaries and the proportion of intergranular fracture during near-threshold fatigue-crack growth at elevated temperatures in the as-received and grain-boundary-engineered microstructures in ME3.

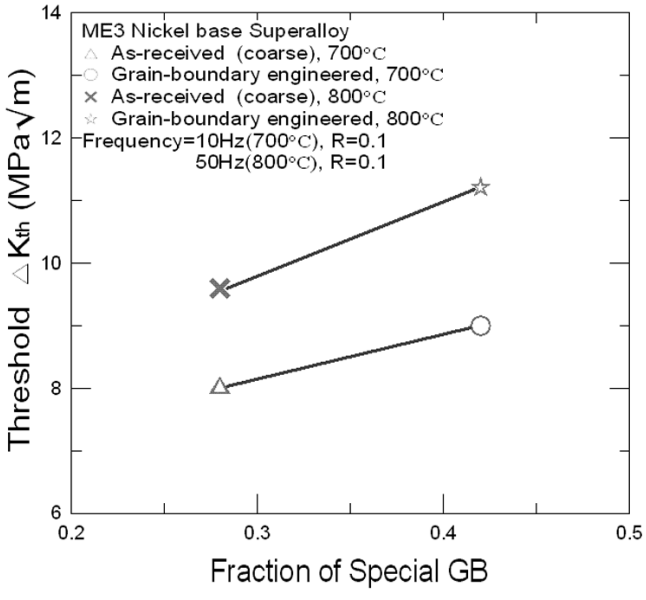

Fig. 9—Relationships between the elevated-temperature ΔK_{TH} fatigue threshold in ME3 tested at 700 °C and 800 °C and fraction of special grain boundaries for the as-received and grain-boundary-engineered microstructures.

annealing (1150 °C for 30 minutes), the number fraction of special grain boundaries in the ME3 microstructure could be increased from 28 to 29 pct to 41 to 42 pct, with little change in crystallographic texture.

2. At a constant grain size, the effect of such an increase in fraction of special boundaries, however, was found to have little influence on the fatigue-crack propagation and ΔK_{TH} threshold behavior of large (~8 to 20 mm) through-thickness at ambient temperatures, primarily because

crack advance in this regime is predominantly transgranular. Fatigue thresholds and near-threshold growth rates, however, were markedly affected by grain size (~1 to 17 μm), with the coarser microstructures displaying significantly better fatigue-crack-growth resistance.

3. At elevated temperatures (700 °C to 800 °C), where near-threshold fatigue-crack propagation comprises ~30 to 75 pct intergranular fracture, the grain-boundary-engineered microstructures were found to show definitively better (large-crack) crack-growth resistance. Specifically, compared to ambient-temperature behavior, the ΔK_{TH} thresholds were ~10 to 20 pct higher, and near-threshold growth rates (at a specific ΔK level) were some 5 to 10 times lower in microstructures with an enhanced fraction of special grain boundaries. Such a beneficial effect on near-threshold crack-growth resistance was attributed to a ~20 to 25 pct reduction in the proportion of intergranular cracking in the grain-boundary-engineered microstructures.

ACKNOWLEDGMENTS

This work was supported by the United States Air Force Office of Scientific Research under Grant No. F49620-02-1-0010. Part of this work was performed under the auspices of the United States Department of Energy by the University of California, Lawrence Livermore National Laboratory, under Contract No. W-7405-Eng-48. The authors thank Drs. Ken Bain and Deborah Demania, GE Aircraft Engines, and Dr. Peter Kantzos, NASA Glenn, for supplying the ME3 alloy; Dr. Velimir Radmilovic, National Center for Electron Microscopy at Berkeley, for extensive help with the microscopy; Lan T. Nguyen for specimen preparation; and Drs. Jamie J. Kruzic and James S. Stölken for several helpful discussions.

REFERENCES

1. *Report of the Ad Hoc Committee on Air Force Jet Engine Manufacturing and Production Processes*, The Pentagon, United States Air Force Scientific Advisory Board, SAF/QQS, Washington, DC, 1992.
2. B.A. Cowles: *Int. J. Fract*., 1996, vol. 80, pp. 147-63.
3. *Proc. 3rd, 4th, 5th and 6th Nat. Turbine Engine High Cycle Fatigue Conf*., J. Henderson, ed., Universal Technology Corp., Dayton, OH, 1998-2001.
4. T. Nicholas and J.R. Zuiker: *Int. J. Fract*., 1996, vol. 80, pp. 219-35.
5. R.O. Ritchie, D.L. Davidson, B.L. Boyce, J.P. Campbell, and O. Roder: *Fatigue Fract. Eng. Mater. Struct*., 1999, vol. 22, pp. 621-31.
6. S.A. Padula, A. Shyam, R.O. Ritchie, and W.W. Milligan: *Int. J. Fatigue*, 1999, vol. 21, pp. 725-31.
7. R.K. Nalla, B.L. Boyce, J.P. Campbell, J.O. Peters, and R.O. Ritchie: *Metall. Mater. Trans. A*, 2002, vol. 33A, pp. 899-918.
8. A.E. Giannakopoulos, T.C. Lindley and S. Suresh: *Acta Mater*., 1998, vol. 46, pp. 2955-68.
9. T. Watanabe: *Res. Mech*., 1984, vol. 11, pp. 47-84.
10. H. Grimmer, W. Bollmann, and D.H. Warrington: *Acta Cryst. A*, 1974, vol. 30A, pp. 197-207.
11. D.G. Brandon, B. Ralph, S. Ranganathan, and M.S. Wald: *Acta Metall*., 1964, vol. 12, pp. 813-21.
12. M. Kumar, A. Schwartz, and W. King: *Acta Mater*., 2002, vol. 50, pp. 2599-2612.
13. B. Bennett and H. Pickering: *Metall. Mater. Trans. A*, 1987, vol. 18A, pp. 1117-24.
14. G. Palumbo and K.T. Aust: *Scripta Metall*., 1988, vol. 22, pp. 847-52.
15. G. Palumbo and K.T. Aust: *Acta Metall. Mater*., 1990, vol. 38, pp. 2343-52.
16. G. Palumbo, P.J. King, K.T. Aust, U. Erb, and P.C. Lichtenberger: *Scripta Metall. Mater*., 1991, vol. 25, pp. 1775-80.
17. D.C. Crawford and G.S. Was: *Metall. Trans. A*, 1992, vol. 23A, pp. 1195-1206.
18. P. Lin, G. Palumbo, U. Erb, and K.T. Aust: *Scripta Metall. Mater*., 1995, vol. 33, pp. 1387-92.
19. G. Palumbo and K.T. Aust: *Can. Metall. Q*., 1995, vol. 34, pp. 165-73.
20. E.M. Lehockey, G. Palumbo, P. Lin, and A.M. Brennenstuhl: *Metall. Mater. Trans. A*, 1998, vol. 29A, pp. 387-96.
21. J. Don and S. Majumdar: *Acta Metall*., 1986, vol. 34, pp. 961-67.
22. D.P. Field and B.L. Adams: *Acta Metall. Mater*., 1992, vol. 40, pp. 1145-57.
23. V. Thaveeprungsriporn and G.S. Was: *Metall. Mater. Trans. A*, 1997, vol. 28A, pp. 2101-12.
24. E.M. Lehockey, G. Palumbo, P. Lin, and A.M. Brennenstuhl: *Scripta Mater*., 1997, vol. 36, pp. 1211-18.
25. E.M. Lehockey, G. Palumbo, and P. Lin: *Metall. Mater. Trans. A*, 1998, vol. 29A, pp. 3069-79.
26. E. Nembach and G. Neite: *Progr. Mater. Sci*., 1985, vol. 29, pp. 177-319.
27. T. Gabb, J. Telesman, P. Kantzos, and K. O'Connor: NASA TM-2002-211796, NASA, Washington, DC, 2002.
28. *Annual Book of ASTM Standards*, *E647*, ASTM, West Conshohocken, PA, 2001.
29. *Annual Book of ASTM Standards*, *E399*, ASTM, West Conshohocken, PA, 1997.
30. M. Kumar, W. King, and A. Schwartz: *Acta Mater*., 2000, vol. 48, pp. 2081-91.
31. A. Schwartz, M. Kumar, and W. King: *MRS Symp. Proc*., 2000, vol. 586, p. 3.
32. C.A. Schuh, M. Kumar, and W. King: *Acta Mater*., 2003, vol. 51, pp. 687-700.
33. C.A. Schuh, M. Kumar, and W.E. King: *Z. Metallkd*., 2003, vol. 94, pp. 323-28.
34. Y. Gao, J.S. Stölken, M. Kumar, and R.O. Ritchie: *Acta Mater*., 2005, in review.
35. R. Molins, G. Hochstetter, J.C. Chassaigne, and E. Andrieu: *Acta Mater*., 1997, vol. 45, pp. 663-74.
36. B. Alexandreanu, B.H. Sencer, V. Thaveeprunsriporn, and G. Was: *Acta Mater*., 2003, vol. 51, pp. 3831-48.
37. M. Kumar, K. Blobaum, J.S. Stölken, and R.W. Minich: unpublished research.